Eur. Phys. J. B **13**, 707–714 (2000)

**THE EUROPEAN PHYSICAL JOURNAL B**

EDP Sciences


# Application of the wavelet transform in the laminar turbulent transition for a flow in a mixed convection phenomenon

C. Abid[a], C. Barberi Moine, and F. Papini

Institut Universitaire des Systèmes Thermiques Industriels[b], Université d'Aix-Marseille 13453, Marseille Cedex 13, France

Received 30 March 1998 and Received in final form 28 April 1999

**Abstract.** The aim of this paper is to show the effect of secondary flows caused by natural convection on the laminar-turbulent hydrodynamic transition. It is not a question of measuring a critical threshold value of Reynolds number of transition but only to estimate the degree of turbulence in the transition regime, *i.e.* weak turbulence in the case of superposition (mixed convection) or not (forced convection) of secondary flows on the forced flow. This is possible thanks to the application of the wavelet transform. The calculation of the Hölder exponent, associated with the maximum value of the singularity spectrum for two configurations, vertical (forced convection) and horizontal (mixed convection) allows the degree of turbulence to be measured in both cases. The variation of the Hölder exponent *versus* the Reynolds number has enabled it to be shown that the secondary flows stabilise the main flow and stifle the beginnings of the turbulence during the regime of transition to turbulence; these kinds of results have also been shown in literature. Generally, large-sized secondary flows (for example Dean's flows) stabilise the turbulence. Our work confirms this, through an experiment carried out in identical conditions for mixed convection (horizontal flow) and forced convection (vertical flow).

**PACS.** 47.27.Cn Transition to turbulence – 02.50.-r Probability theory, stochastic processes, and statistics – 05.40.-a Fluctuation phenomena, random processes, noise, and Brownian motion

## 1 Introduction

The hydrodynamic laminar-turbulent transition, for forced internal flows, has been the subject of many studies which show the regime to be sensitive to experimental conditions (geometry, roughness of the wall, inlet conditions). These studies, for which we give some essential bibliographical references without seeking to be exhaustive [1–5], have mainly aimed at determining the critical Reynolds number for different experimental conditions and the wall-fluid heat transfer, and studying the hydrodynamic instabilities. In the particular case where the wall is heated, each gravity component perpendicular to the main flow induces a secondary circulation with a maximum effect for the horizontal position of the duct. This type of flow is encountered in various industrial applications sometimes presenting process problems as a result of strong temperature gradients in a straight section. However, in this case, the global wall-fluid heat transfer is greatly improved in relation to pure forced convection [7,8], particularly in a laminar regime. These secondary flows also influence the laminar-turbulent transition; thus two ways of transition to the turbulence have been evidenced [8]: hydrodynamic, controlled by the Reynolds number and thermal, controlled by the Rayleigh number; both ways may be coupled, if these control parameters take on sufficiently high values. To characterise the hydrodynamic transition more specifically Petukhov *et al.* [9] evaluate the variation of the intermittence rate for the temporal signal which corresponds to the wall temperature, *versus* the Reynolds number; they compare their results to those of Rotta [2] obtained by the same process but from local time variations of the fluid velocity, as the flow is isothermic (without a heat supply); they also show that natural convection delays the turbulence during this hydrodynamic transition.

Our study concerns this hydrodynamic transition for the mixed convection phenomenon. We will compare the arrival of turbulence in the case of pure forced convection (no gravity effect, pure Poiseuille flow) and the case of mixed convection (superposition of secondary flows on the main flow) by estimating the degree of turbulence in both situations. Thus, we work with a flow in a cylindrical duct, heated at the wall and able to pass from the vertical position (which corresponds to forced convection) to the horizontal position (mixed convection) with all the other experimental parameters maintained.

For such an analysis, the information used is the temperature measured on the external wall. The corresponding temporal signal processing technique is the wavelet transform. By bringing times and frequencies into operation simultaneously, this transformation may prove

[a] e-mail: ca@iusti.univ-mrs.fr
[b] UMR CNRS 6995

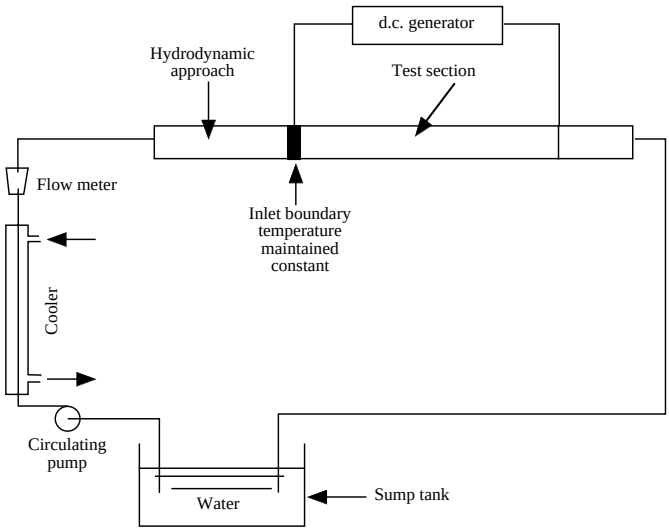


**Fig. 1.** Diagram of experimental loop.

particularly suited and efficient as the recent studies of the turbulent regime elsewhere have shown [10,11]. Our conclusions will essentially be based on the comparison of the Hölder exponent associated with the maximum value of the singularity spectrum. In the transition zone at the same Reynolds number for both configurations, the value of the Hölder exponent enables the degree of turbulence in both configurations to be estimated and thus the effect of the presence of secondary flows on turbulence development in this transition regime to be quantified.

## 2 Experimental set-up

Our experiments concern the study of the flow of a monophasic fluid (water) in a horizontal or vertical cylindrical tube heated uniformly at the wall. The experimental set-up is presented in Figure 1. The tube is in inconel 0.2 mm thick. The outside diameter is 1 cm and the total length 2 m. The 1 m central zone, which is not insulated from the environment, corresponds to the testing zone (the aspect ratio is thus equal to 100). The first part of the tube (before the testing zone) enables the fluid to be established hydraulically so that the flow is Poiseuille type at the inlet of this zone. Moreover, it is free at the outlet. The fluid circulation is ensured by a multistage centrifugal pump (rotation 2800 r.p.m). The average fluid velocity $v$ is regulated by a flowmeter. The fluid passes through a heat exchanger before entering the section, in order to ensure a constant inlet temperature. The testing zone wall (whose electrical resistance is 0.16 ohm) is heated electrically by applying a direct electric current between the input and output terminals; the strength may vary from 10 to 75 A s. The input terminal is maintained at a constant temperature by an external fluid circulation. The heat flux $P$ is uniform on the straight section throughout the testing zone and is of an order of 20 kW/m$^2$ (for a 65 A current); taking into account the temperature values reached, the external heat losses of the tube are around 500 W/m$^2$ (that is 2% of $P$). The inlet of this zone is taken as the origin of the axial coordinate $z$.

In order not to perturb the flow, no measurement is carried out in the fluid. For a given fluid velocity and heat flux, the temperature field is measured on the external wall. In the experiments presented, this measure is carried out by means of a type K thermocouple 0.2 mm in diameter applied to the wall at axial coordinate $z =$ 80 cm. The signal sampling time step is 0.02 s and the measurement accuracy is around 0.1 °C.

## 3 Experimental results

The flow in a horizontal tube heated at the wall reveals a temperature difference between the top and the bottom of a straight section in a stable laminar regime. For example [12], for a heat flux of 20 kW/m$^2$ and a Reynolds number of 750 this difference can reach 40 °C at an axial coordinate $z = 80$ cm. The Reynolds number is calculated by considering the average fluid velocity $v$ and by estimating the physical properties at the average temperature of the fluid between the inlet and the outlet of the heated zone. The bulk temperature of the fluid, evaluated by an inlet-outlet heat balance, increases from 15 °C at the inlet to 25 °C at the outlet of the heated zone, for a Reynolds number of 2000 and a heat flux of 20 kW/m$^2$. The temperature difference in a straight section is due to the secondary flows created by the effect of gravity which are superposed on the main axial flow; these flows are composed of two contrarotating rolls which are symmetrical in relation to the vertical plane passing through the tube axis [13]. The corresponding velocities increase with axial coordinate $z$, increasing the heat transfer from the bottom to the top of the straight section, which contributes to the increase in the temperature difference.

When the flow velocity (Reynolds number) and/or the heating flux (Rayleigh number) [14–16] is increased, an instability phenomenon appears. Large amplitude fluctuations manifest themselves randomly on the wall temperature. Moreover, an examination of the fluctuations shows that they are always characterised by two time constants. The first, relating to the temperature drop, is of an order of one second, while the other, which corresponds to the return to the stationary state, is around ten seconds. These instabilities are localised on an instability diagram in a *Re-Ra* plane (see Fig. 2). We call these instabilities "thermoconvective instabilities". They are characteristic of the mixed convection phenomenon. For greater values of the two parameters ($Re$ and $Ra$), we distinguish two types of "laminar-turbulent" transition, of hydrodynamic or thermal nature. Two possible ways therefore exist to go towards the turbulence. In this presentation we will only study the hydrodynamic "laminar-turbulent" transition [17]. Thus, we will be concerned with the arrival of the weak turbulence and the role of the transverse secondary flows in this regime.

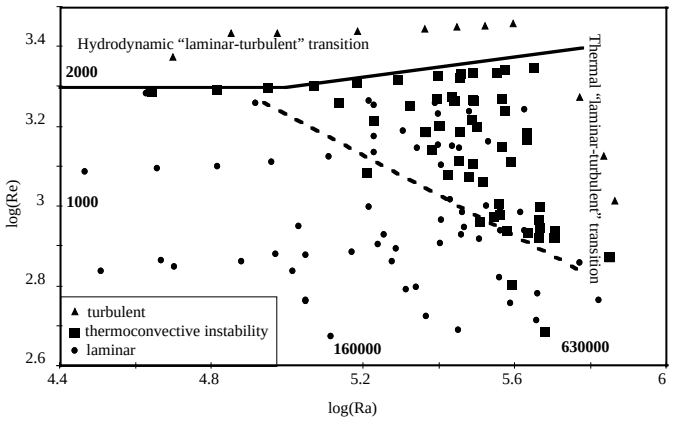


**Fig. 2.** Diagram of stability of the system : $\log(Re)$ *vs.* $\log(Ra)$.

## 4 Technique of analysis

### 4.1 Wavelet transform

The analysis of most signals generally involves the use of the Fourier transform. Although this technique is efficient for analysing stationary phenomena, it is inefficient in the case of non-stationary signals. The wavelet transform was introduced in order to remedy this [18,19]. This wavelet transform enables the signal to be decomposed both into time and into scales; the signal is thus no longer represented with frequency components but with a linear combination of elementary functions. These functions are constructed by expanding and translating a single function $g$. The wavelet transform of a signal $s(x)$ is thus written:

$$T_g[s](a,b) = \frac{1}{a}\int_{-\infty}^{+\infty} s(x)\bar{g}\left[\frac{x-b}{a}\right]\mathrm{d}x \quad \text{with} \quad a>0 \tag{1}$$

where $a$ is a scale parameter and $b$ a translation parameter of the wavelet.

The mother wavelet $g$ must satisfy an admissibility condition. Let us note that this implies that $\hat{g}(0)=0$ and therefore, if $g \in L'(\Re)$,

$$\int_{-\infty}^{+\infty} g(x)\mathrm{d}x = 0. \tag{2}$$

A mother function $g$ which satisfies equation (2) will be called an analysing wavelet.

The choice of analysing wavelet has often been the derivatives of order $N$ of the Gaussian function, that is:

$$g^{(N)}\Big(x\Big) = \frac{\mathrm{d}^N}{\mathrm{d}x^N}\mathrm{e}^{-\frac{x^2}{2}}. \tag{3}$$

From the maximum of the wavelet transform module a partition function may be constructed which, on one hand, only covers the singular parts of the signal and, on the other, measures the local Hölder exponent. Arnéodo *et al.* [20–24] suggest using the following formulation:

$$Z(q,a) = \sum_{l\in L(a)} \left(\sup_{\grave{a}\le a}|T_g[s](b_l(\grave{a}),\grave{a})|^q\right)$$
$$Z(q,a) \approx a^{\tau(q)} \tag{4}$$

where $L(a)$ is the set of all the maxima lines of $T_g[s]$ which exist on the scale $a$, and $b_l(a)$ is the position of the maximum of the line $l$ module on this scale $a$. It is a scale adaptive partition which will prevent divergences from showing up in the calculation of $Z(q,a)$ for negative $q$ values.

The multifractal formalism developed by Arnéodo *et al.* [24] consists in computing the singularity spectrum $D(h)$ of a function $s$ as the Legendre transform of the function $\tau(q)$, that is:

$$D(h) = \min_q[qh - \tau(q)]. \tag{5}$$

This approach is generally called the wavelet transform module maxima method (WTMM). The $h(q)$ and $d(q)$ entities may also be defined by means of a canonical definition:

$$h(q,a) = \sum_{l\in L(a)} \hat{T}_g[s](q,l,a)\ln|\sup_{\grave{a}\le a}T_g[s](b_l(\grave{a}),\grave{a})|$$
$$D(q,a) = \sum_{l\in L(a)} \hat{T}_g[s](q,l,a)\ln|T_g[s](q,l,a)| \tag{6}$$

with: $\hat{T}_g[s](q,l,a) = |\sup_{\grave{a}\le a}T_g[s](b_l(\grave{a}),\grave{a})|$.

The $D(h)$ spectrum is obtained by representing $D(q)$ *versus* $h(q)$ for different values of $q$.

From these definitions, we have developed an algorithm which allows the different resulting magnitudes of the wavelet transform to be determined. The algorithm used to determine singularity spectra and Hölder exponents may be divided into two parts :

- calculation of the wavelet transform of the considered signal and calculation of local maxima of the module,
- calculation of the partition functions and evaluation of functions $h(q,a)$ and $D(q,a)$.

The calculation of spectra $D(h)$ and $\tau(q)$ may be done by means of canonical functions, as an alternative to the Legendre transform.

### 4.2 Validation

In order to validate our calculation tool, it is tested on signals for which spectrum $D(h)$ may be expressed analytically. We choose a "devil's staircase" type monofractal signal associated with the analytically determined "triadic Cantor". The partition functions $Z(q,a)$ are computed from the WTMM. The $\tau(q)$ spectrum follows a linear curve, the slope of which provides an estimate of the unique Hölder exponent $h$ = Log 2/Log 3, which characterises the uniform triadic Cantor set. The singularity spectrum is reduced to a single point $D(h =$ Log 2/Log 3) = Log 2/Log 3, *i.e.*, the Hausdorff dimension of the triadic set [22].

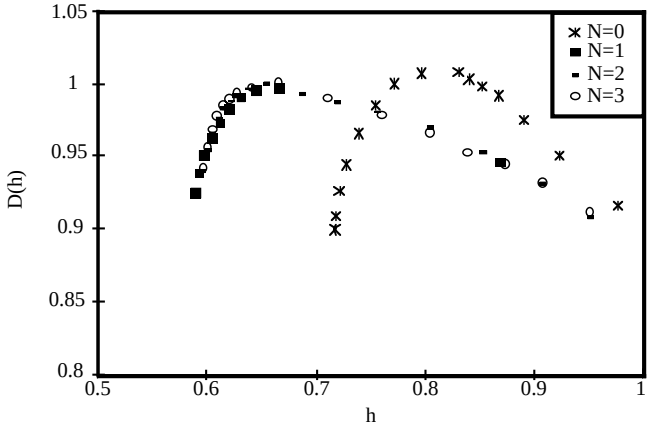


**Fig. 3.** WTMM measurement of the singularity spectrum of an experimental signal for various order $N$ of the derivative Gaussian function as an analysing wavelet.

## 5 Application to experimental signals

### 5.1 Precautions

Before applying the WTMM method to the experimental signals, a certain number of precautions must be considered.

#### 5.1.1 Signal dynamics

Firstly, it is necessary to check that the signal dynamics and the acquisition time resolution are sufficient to avoid bias in the results. We therefore limited our investigation to a range of Reynolds numbers from 2000 to 4000.

Indeed, at low Reynolds numbers, we find ourselves in the thermoconvective instability zone, that is, signals containing stationary phases, of variable duration, interrupted by large amplitude fluctuations [14,15]. The corresponding signal contains great irregularities due to very localised structures. To analyse these signals another procedure should be adopted, such as that applied for pressure signal processing recorded by the Couder group [25].

In the case of high Reynolds numbers, the signal amplitude becomes low and the signal is no longer represented on scales significantly enough to be analysable by the wavelets.

#### 5.1.2 Choice of the analysing wavelet

The analysing wavelet $g$ is generally chosen to be well localised in both space and frequency. The Gaussian derivatives are tested up to order 4. For a given signal, Figure 3 shows the evolution of the singularity spectrum $D(h)$. It is to be noted that the spectrum given by the analysing function of a non zero average, *i.e.*, the Gaussian curve, differs completely from the other spectra. However, from $N = 1$, the spectra are practically imperceptible and are therefore now independent of the chosen analysing wavelet in so far as the latter is orthogonal to the constants. This analysis thus suggests the presence of smooth behaviours, low frequency in the signal causing broken invariance. As the choice of the analysing wavelet is flexible, the WTMM allows us to avoid the low frequency behaviour. So, as from the first derivative of the Gaussian curve, as analysing wavelet, the results may be said to be non biased. The second derivative of the Gaussian "Mexican hat" is therefore chosen as the analysing wavelet.

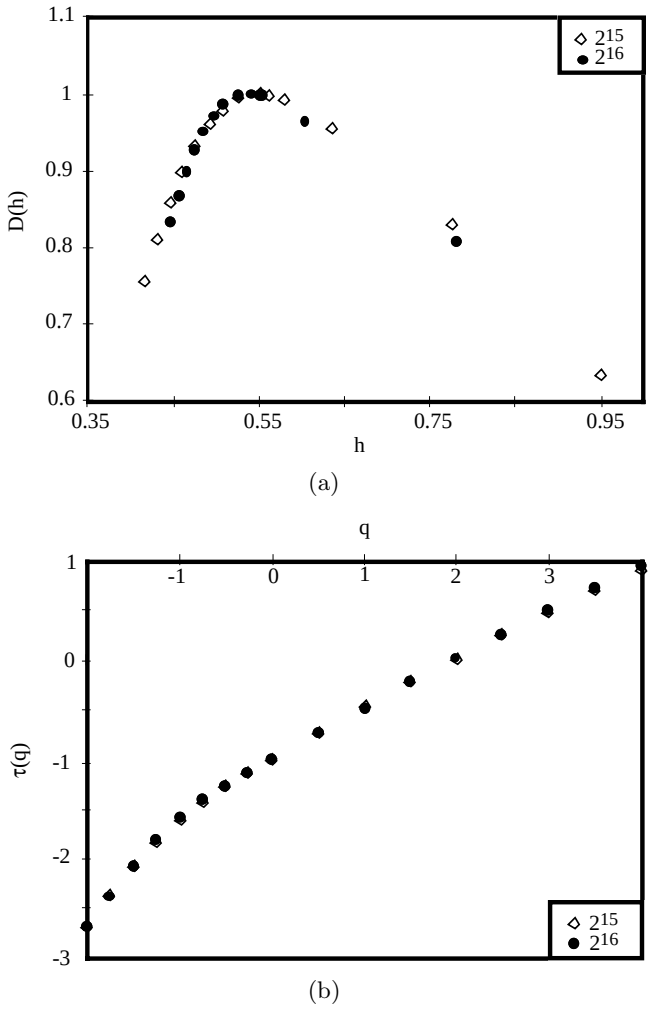


**Fig. 4.** WTMM measurement of the singularity spectrum, (a) $D(h)$ *vs.* $h$ and (b) $\tau(q)$ *vs.* $q$, for two different lengths of signals.

#### 5.1.3 Evolution versus the signal length

The maximum duration of a recording is around 7 hours, which corresponds to a total file of 1 600 000 values. From this file, we build up the different realisations to be processed. An analysis is carried out in relation to the length of realisation. For this, we consider two different lengths of realisation, that is $2^{15}$ and $2^{16}$ values, and we apply the WTMM method. Then, for an average of ten realisations we determine the singularity spectrum $D(h)$ as well as the function $\tau(q)$ for both cases. As an example, Figure 4 shows the evolution of $D(h)$ and of $\tau(q)$ for lengths of $2^{15}$ and $2^{16}$ values for a given experimental signal. There does not seem to be an evolution between these two lengths

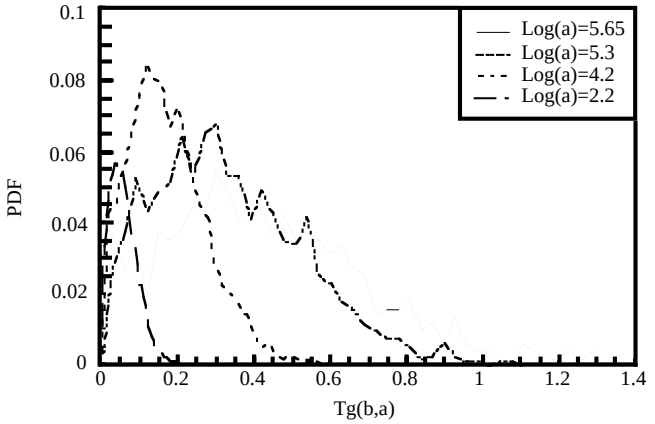


**Fig. 5.** Probability distribution functions for various scales $a$.

and therefore processing on files of $2^{16}$ values may be considered sufficient for the range of Reynolds numbers under consideration. Moreover, comparing an average from ten or twenty realisations, the average does not evolve and it can be considered that ten realisations are sufficient for statistics.

### 5.1.4 Evolution of distribution functions and moments

The distribution functions are determined by evaluating the moments of the order $q$ of the wavelet coefficients when $a$ and $q$ vary. Established statistics for these moments must not present bias nor distortion which could render the summation result too erroneous. For a fixed length of signal, the distribution functions are therefore to be analysed with care, in order to retain only the interval of values of $a$ and $q$ for which the resulting error is permissible. This allows us firstly to determine the scale range $a$ on which the linear regressions may be made and secondly to limit the value range of $q$, which may be scanned to calculate the partition functions $Z(q, a)$. As an example, for a given experimental signal, the probability distribution functions (PDF) are shown in Figure 5, calculated from the maxima for different scale values $a$. It is to be noted that when the scale decreases, the PDF tends to be concentrated on the low values of the wavelet coefficients. This behaviour leads to great inaccuracies for moments of order $q$, while $q$ is negative. When scale a increases, the PDF becomes more and more irregular, especially for high values of the wavelet coefficients, which may lead to statistical problems for moments of order $q$ when $q$ is positive.

However, another limitation is called for. Indeed, the limits of the values of $q$ must be determined to calculate moments of order $q$. Thus, for a scale $\log(a) = 5.65$, the curves allowing the computing of the moments of order $q$ are displayed in Figure 6. For positive values of $q$, it is to be noted that when the value of $q$ increases, integration is carried out more and more on the fluctuation to be found around the great wavelet coefficients values. When $q$ decreases, the integration area is concentrated on the small wavelet coefficient values. These two aspects imply distortions and bias on the calculations done.

The probability distribution function curves and moments of order $q$ allow reasonable limits of the parameter

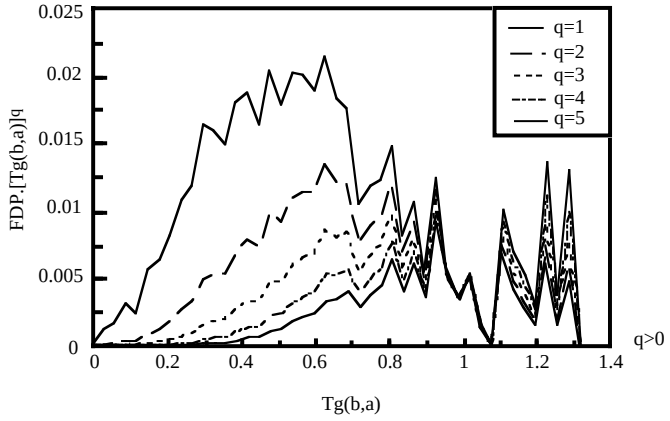


(a)

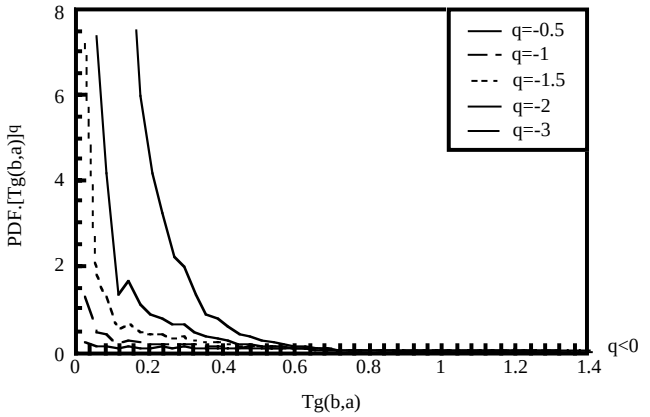


(b)

**Fig. 6.** Curves for computing moments of order $q$ for various $q$ values ($\log(a) = 5.65$).

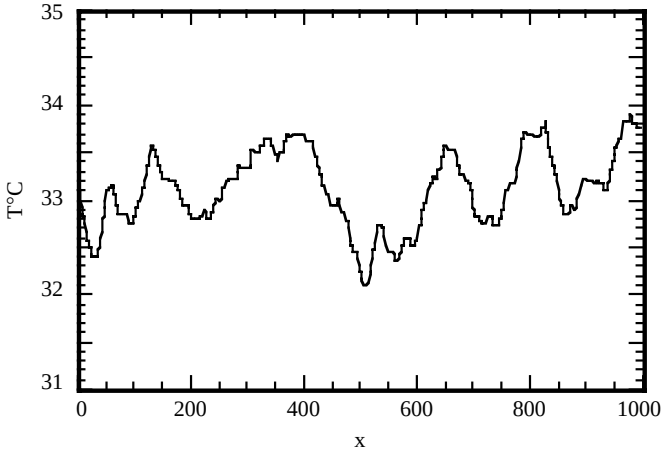


**Fig. 7.** Evolution of the temperature signal ($Re = 3400$ and $P = 21.5$ kW/m$^2$).

values $a$ and $q$. The limits adopted, for the fixed length of realisation, are such that:

- regression range: $2 < \log a < 6$
- moments order $q$: $-1.5 < q < 4$

outside these intervals, the biases will be too great and the corresponding results invalid.

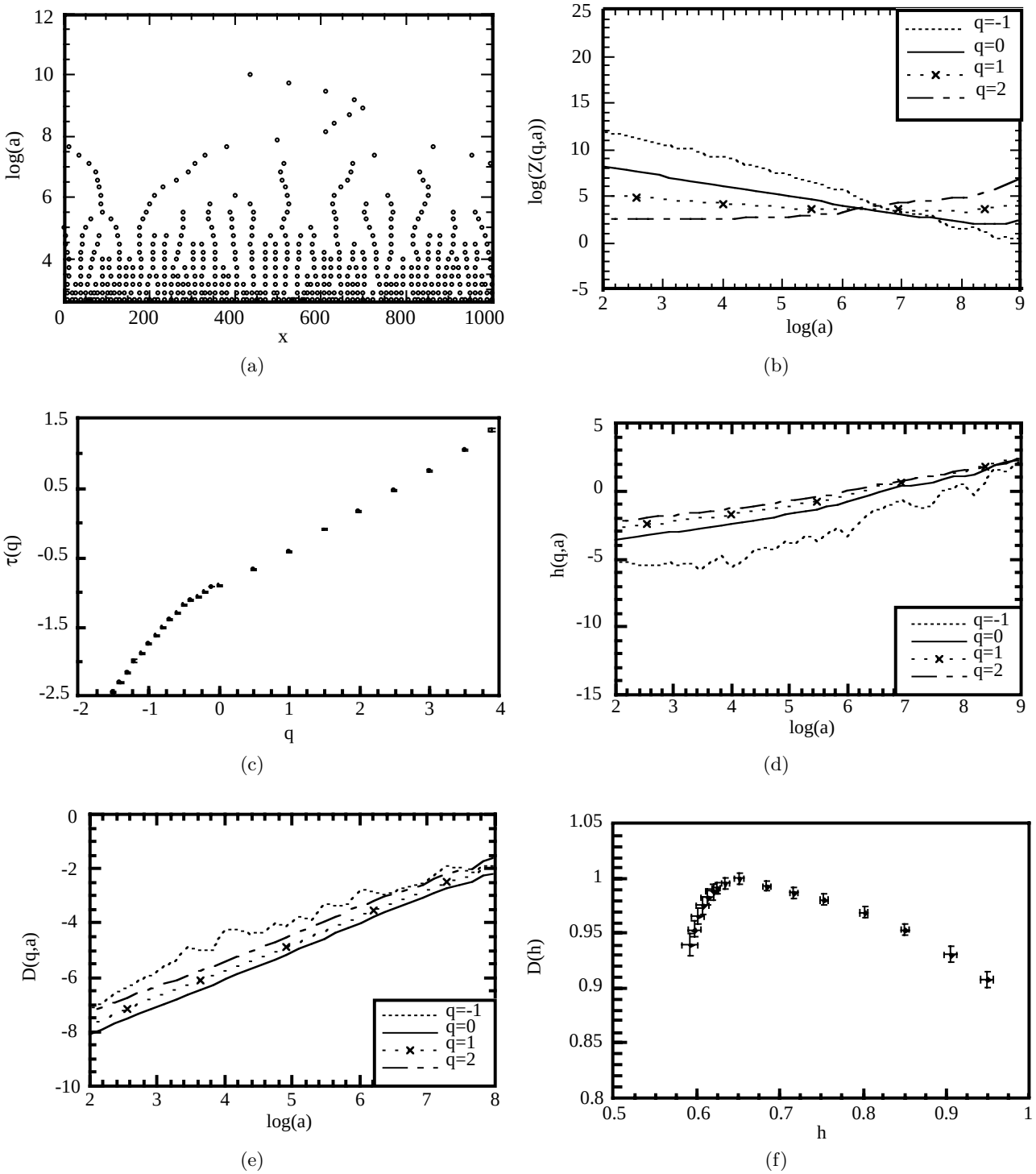


**Fig. 8.** WTMM measurement of the signal shown in Figure 7, (a) WT skeleton of the modulus maxima of $T_g$, (b) $\log Z(q,a)$ *vs.* $\log(a)$, (c) $\tau(q)$ *vs.* $q$, (d) $h(q,a)$ *vs.* $\log(a)$, (e) $D(q,a)$ *vs.* $\log(a)$, (f) $D(h)$ *vs.* $h$.

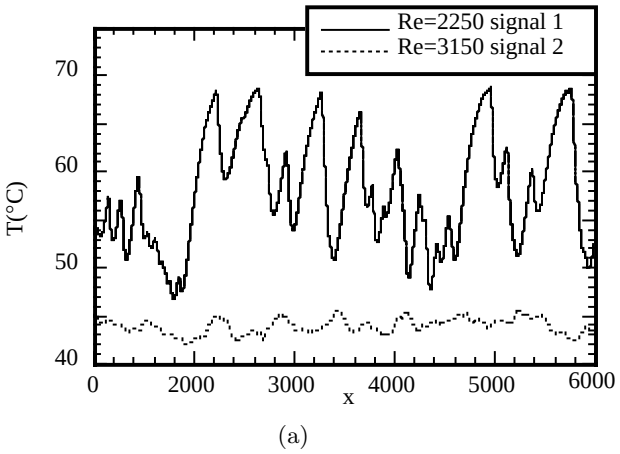


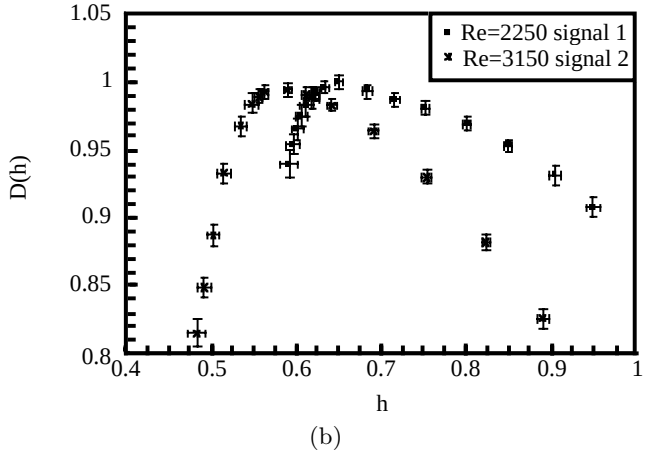


**Fig. 9.** WTMM measurement for two different Reynolds numbers, (a) graph of signals, (b) $D(h)$ *vs.* $h$.

### 5.2 Results

Having described the WTMM method, we will now apply this technique to the experimental signals. These signals concern the evolution of the wall temperature, at the top of a straight section, at an axial coordinate $z = 80$ cm for a heat flux $P = 21.5\ \mathrm{kW/m^2}$. As an example Figure 7 shows the evolution of a temperature signal for a Reynolds number $Re = 3400$. The corresponding wavelet transform modulus maxima skeleton computed with the "mexican hat" is illustrated in Figure 8a. In Figure 8b various curves of $\log_2 Z(q,a)$ *versus* $\log_2(a)$ are displayed for various values of $q$. A linear behaviour is observed (on the scale range observed) for all the values of $q$. The exponent $\tau(q)$ extracted from the power-law behaviour of $Z(q,a)$ is represented in Figure 8c. $\tau(q)$ is an increasing convex nonlinear function of $q$. Figure 8d displays various curves $h(q,a)$ *versus* $\log_2(a)$ whose slope permits us to estimate $h(q)$. The slope of the functions $D(q,a)$ (Fig. 8e) represented *versus* $\log_2(a)$, for different values of $q$, gives $D(q)$. By means of $h(q)$ and $D(q)$, we obtain the singularity spectrum $D(h)$ which is displayed in Figure 8f. The maximum value of $D(h)$ is equal to $0.99 \pm 0.1$; this value suggests that the signal is almost everywhere singular. In this figure, it can be seen that the singularity encountered most frequently (the one which corresponds to the maximum of $D(h)$) is of the Hölder exponent $h = 0.65 \pm 0.01$. *A priori*, the aspect of the spectrum may suggest that the signal is not monofractal. However, the limited spread of the values does not reveal an obvious multifractal aspect either.

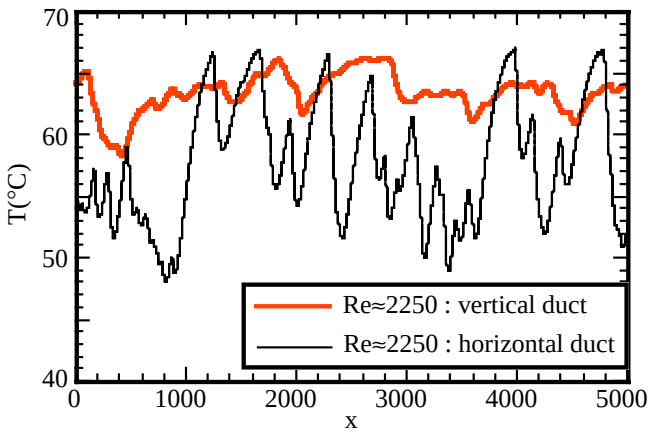


**Fig. 10.** Evolution of the temperature signal for vertical and horizontal configurations ($Re = 2250$).

The control parameter of the hydrodynamic laminar-turbulent transition is the Reynolds number; we therefore apply the WTMM to temperature signals corresponding to the values of the fluid velocity concerning this regime (Reynolds numbers between 2000 and 4000). Thus, Figure 9a shows the evolution of the wall temperature signal for two different values of the Reynolds number, in the studied range. As the shape of the various intermediate magnitudes to determine the spectrum $D(h)$ are similar to those of the previous example, we confine ourselves to representing simply the singularity spectrum $D(h)$ concerning the two signals (see Fig. 9b). The same observations (example Fig. 8) remain valid. However, the value of exponent $h$ associated to the maximum of spectrum $D(h)$, marked $h_{\max D(h)}$, decreases when the Reynolds number increases; indeed, in the case of signal 1 ($Re = 2250$) $h_{\max D(h)}$ is evaluated at $0.65 \pm 0.01$; in the case of signal 2 ($Re = 3150$), $h_{\max D(h)}$ is evaluated at $0.59 \pm 0.01$. This result is foreseeable since this Hölder exponent must go to value $1/3$ when the fully developed turbulence is reached, which complies with Kolmogorov's theory [11].

We exploit this property, that is the evolution of $h_{\max D(h)}$, essentially to evaluate the degree of turbulence of a given signal. Thus, to appreciate the effect of the secondary flows, caused by natural convection, on the hydrodynamic "laminar-turbulent" transition, we propose to evaluate $h_{\max D(h)}$ during this transition in the cases of a configuration without secondary flows, *i.e.*, pure forced convection and of a configuration with secondary flows *i.e.* mixed convection.

In the same range of the Reynolds number ($Re \approx 2000$ to 4000) considering the same axial coordinate $z$ and the same heat flux supplied to the wall, we record signals of the wall temperature evolution, for the horizontal (mixed

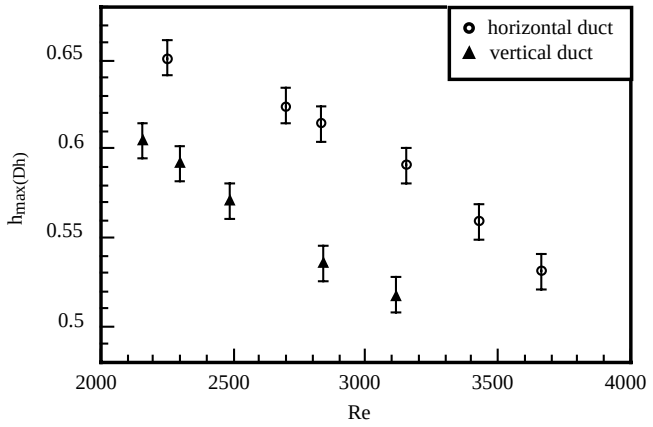


**Fig. 11.** Variation of the $h_{\max(D(h))}$ *versus* the Reynolds number for both the horizontal and the vertical duct.

convection) and vertical (forced convection) configurations. To illustrate this, Figure 10 shows the evolution of the signal for both configurations for the same value of the Reynolds number. Considering the same statistics, we apply the WTMM for the various recorded signals and calculate the corresponding Hölder exponent $h_{\max D(h)}$. Figure 11 shows that the $h_{\max D(h)}$ follow parallel evolutions in both configurations *versus* the Reynolds number and that the values of $h_{\max D(h)}$ for the vertical tube (forced convection) are situated below those for the horizontal tube (mixed convection). This shows that the degree of turbulence is greater in forced convection than in mixed convection. In this case, the secondary flows, caused by natural convection, reduce the turbulence level and play the role of "stabiliser" of the weak turbulence. The convective rolls structure the flow and stifle the beginnings of the turbulence. It could be said that the movement carried by natural convection is coherent and that this coherent movement controls the first incoherent nuclei of the turbulence in the presence of weak turbulence in the system.

## 6 Conclusion

The use of the wavelet transform for thermal signals enables us to characterise the hydrodynamic "laminar-turbulent" transition. The comparison of the results under the same experimental conditions obtained for a vertical (forced convection) and a horizontal mixed convection flow shows the effect of transverse secondary flows in this regime. Essentially, we note that the latter play a stabilising role in relation to the advent of the turbulence and thus delay the hydrodynamic transition. This conclusion is possible thanks to the use of the variation of the Hölder exponent associated to the maximum value of the singularity spectrum *versus* the Reynolds number.

The authors acknowledge A. Arnéodo, Directeur de Recherches au CNRS (Centre de Recherche Paul Pascal, Université de Bordeaux, Talence), for his profitable advice during the elaboration of this work, especially concerning the use and implementation of the WTMM method.

## References

1. O. Reynolds, Phil. Trans. Roy. Soc. **174**, 935 (1883).
2. J. Rotta, Ing.-Arch. **24**, 258 (1956).
3. H.L. Dryden, ZWF **4**, 89 (1956).
4. H. Schlichting, *Entstehung der turbulenz. Handbuch der Physik 8/1* (Springer-Verlag, 1959), pp. 351-450.
5. W. Tollmien, D. Grohne, in *Boundary layer and flow control* (Pergamon Press, London, 1961), Vol. 2, pp. 602-636.
6. J.T. Stuart, in *Laminar boundary layers*, edited by L. Rosenhead (Clarendon Press, Oxford, 1963), pp. 482-579.
7. H.R. Nagendra, J. Fluid Mech. **57**, 269 (1973).
8. M.A. El-Hawary, J. Heat Transfer **102**, 273 (1980).
9. P.S. Petukhov, A.F. Polyakov, Flow and heat transfer in horizontal tubes under combined effect of forced and free convection, fourth Int. Heat Transfer, NC3.7, 1-11 (1970).
10. E. Bacry, A. Arnéodo, U. Frich, Y. Gagne, E.J. Hopfinger, in *turbulence and coherent structures*, edited by M. Lesieur, O. Metais (Kluwer Academic Publishers, 1989).
11. E. Bacry, Transformation en ondelettes et turbulence pleinement développée, Rapport de Magistère, Univ. Paris VII, 1989.
12. C. Abid, La convection mixte dans un conduit horizontal : Instabilités thermiques dans la transition "laminaire - turbulent", thèse de doctorat, Marseille, 1993.
13. C. Abid, F. Papini, A. Ropke, D. Veyret, Int. J. Heat Mass Transfer **37**, 91 (1994).
14. C. Abid, F. Papini, A. Ropke, J. Phys. III France **3**, 255 (1993).
15. C. Abid, F. Papini, Int. J. Heat Mass Transfer **40**, 1863 (1997).
16. C. Abid, F. Papini, Phys. Rev. E **56**, 6735 (1997).
17. C. Barberi-Moine, Analyse de distributions fractales à l'aide de la transformée en ondelettes dans la transition laminaire-turbulent en convection mixte, thèse de doctorat, Marseille, 1997.
18. J. Morlet, NATO ASI series, vol. FI (Springer, Berlin, 1983).
19. A. Grossmann, J. Morlet, S.I.A.M. J. Math. Anal. **15**, 723 (1984).
20. J.F. Muzy, E. Bacry, A. Arnéodo, Phys. Rev. Lett. **67**, 3515 (1991).
21. J.F. Muzy, E. Bacry, A. Arnéodo, Phys. Rev. E **47**, 875 (1993).
22. E. Bacry, A. Arnéodo, J.F. Muzy, J. Stat. Phys. **70**, 635 (1993).
23. J.F. Muzy, Analyse de distributions fractales à partir de leur transformée en ondelettes : des concepts mathématiques aux applications physiques, thèse de doctorat, Nice, 1993.
24. A. Arnéodo, F. Argoul, E. Bacry, J. Elezgaray, J.F. Muzy, *Ondelettes, multifractales et turbulences* (Diderot Editeur, 1995).
25. O. Cadot, S. Douady et Y. Couder, Phys. Fluids A **7**, 630 (1995).